Lack of support for adaptive superstructure $NiPt_7$: Experiment and first-principles calculations

B. Schönfeld,[1] M. Engelke,[1] and A. V. Ruban[2]
[1]*Department of Materials, Laboratory of Metal Physics and Technology, ETH Zurich, 8093 Zurich, Switzerland*
[2]*Department of Materials Science and Engineering, KTH, Stockholm, Sweden*
(Received 9 October 2008; published 2 February 2009)

Order and effective interaction parameters on the Pt-rich side of solid Ni-Pt alloys have been investigated by experimental and first-principles theoretical techniques. Diffuse x-ray scattering was taken from single-crystalline Ni-87.8 at. % Pt aged at 603 K to set up a state of thermal equilibrium. From the separated short-range order scattering, effective pair interaction parameters were determined. These experimentally deduced values do not produce the suggested $NiPt_7$ superstructure at lower temperatures. Instead of that, phase separation into $NiPt_3$ regions with $L1_2$ structure and a Pt-rich matrix is observed in Monte Carlo simulations and supported by x-ray scattering of Ni-75.2 at. % Pt. First-principles calculations at 0 K also show that the suggested $NiPt_7$ phase is unstable against decomposition into $NiPt_3$ and Pt.

DOI: 10.1103/PhysRevB.79.064201 PACS number(s): 61.05.C−, 61.66.Dk, 64.60.Cn

I. INTRODUCTION

Ni-Pt alloys have attracted much interest with respect to their surfaces and their catalytic and structural aspects. Large differences are noted between low-index planes, where the interplanar distances vary largely between the open (110) surface and the close-packed (111) surface. Reconstruction, well known for Pt surfaces, but missing for Ni surfaces, is well established for (100) surfaces of Ni-50 at. % Pt, and not known for the (111) and (110) surfaces. The most striking feature is the segregation reversal, i.e., instead of a Pt enrichment in the top layers of (100) and (111) surfaces, a Ni enrichment is found for the (110) surface.[1] As has been demonstrated,[2] the essential driving forces for surface segregation reversal is the segregation of Pt into the second layer, which—being accompanied by a strong interlayer ordering—makes the surface segregation of Ni more energetically favorable.

Experimental information of phase equilibria and ordering in bulk Ni-Pt is still limited. Three ordered phases have been reported in this system: Ni_3Pt ($L1_2$ structure below 853 K), NiPt ($L1_0$ structure below 918 K), and $NiPt_3$ ($L1_2$ structure below about 790 K).[3,4] Note that $NiPt_3$ is not included in the phase diagram handbooks of Massalski.[5] Atomic short-range order (SRO) in this system has been investigated in two detailed diffuse scattering experiments, both for alloys close to the 1:1 stoichiometry.[6,7] Using x rays, Saha and Ohshima[6] investigated Ni-50 at. % Pt at room temperature after aging at 1073 K. Strong diffuse maxima at 100 positions were measured consistent with local elements of the $L1_0$ superstructure. No additional maxima were found at $\frac{1}{2}\frac{1}{2}\frac{1}{2}$ positions as for Cu-Pt.[8]

Using thermal neutrons, Rodriguez *et al.*[7] investigated a null-matrix Ni-48 at. % Pt crystal (with the Ni-62 isotope) at room temperature after aging at 973 K. This allows diffuse scattering to be measured close to Bragg positions, as Bragg scattering is close to zero. Also thermal diffuse scattering and Huang scattering that strongly increase toward Bragg reflections are discriminated experimentally. Thus, the central quantity of interest, namely, short-range order scattering, is best accessible. From the separated short-range order scattering, effective pair interaction (EPI) parameters were determined. A fictive quenching temperature deduced to be 21 K below the aging temperature of 973 K was employed as ordering kinetics are too fast to quench in the atomic arrangement present at this aging temperature (the relaxation time for ordering is about 1 s according to Dahmani *et al.*[9]). A direct comparison with the data of Saha and Ohshima[6] is not straightforward because a higher aging temperature was employed, but only the fastest-quenched top 2 μm at the surface are important in the x-ray measurement, in contrast to the millimeter bulk range with neutrons.

There are several first-principles-based studies of the thermodynamic properties, phase stability, and ordering behavior in Ni-Pt,[10–14] where the electronic origin of the ordering has been investigated. Recently, it was suggested by Sanati *et al.*,[15] on the basis of first-principles calculations of the concentration-independent effective cluster interaction (ECI) parameters for the enthalpies of formation, that an ordered tetragonal $NiPt_7$ phase should be formed below 371 K, in addition to the three ordered structures Ni_3Pt, NiPt, and $NiPt_3$ (Fig. 1). Long-range strain arising from the stacking of size-mismatched Ni and Pt enriched planes was identified to be responsible for the stability of this adaptive structure.

It is the object of this work to investigate the stability of the suggested $NiPt_7$ superstructure. For this to achieve first-

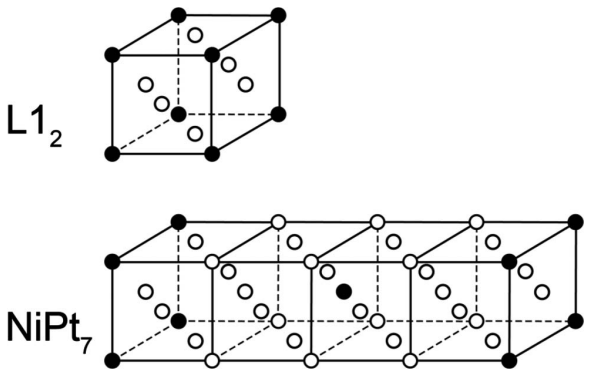

FIG. 1. Crystal structures of ground states that are considered for Pt-rich Ni-Pt, $L1_2$ ($NiPt_3$), and $NiPt_7$.

principles theoretical and diffuse-scattering experimental techniques were performed. The diffuse scattering was done for a state of thermal equilibrium from a solid solution close in composition to the stoichiometry of the suggested $NiPt_7$ structure. This is expected to minimize any dependence on temperature and composition that may affect the EPI parameters deduced from diffuse scattering. Total-energy calculations were done at 0 K to investigate the stability of $NiPt_7$. To provide a comparison with EPI parameters from diffuse scattering, ECI parameters at elevated temperature were also determined from first-principles calculations.

II. METHODOLOGY

Prior to the diffuse scattering experiment, the ordering kinetics were investigated to set up a state with a high degree of local order by aging at a sufficiently low temperature where kinetics are still sufficiently fast to reach a state of thermal equilibrium. Mo $K\alpha$ instead of Cu $K\alpha$ radiation (as in Ref. 6) was employed, which helps to reduce the sensitivity to surface preparation artifacts in an x-ray experiment.

A. Diffuse scattering technique

The elastic diffuse scattering I_{diff} from crystalline solid solutions originates from any static deviation of the actual lattice site from the corresponding one of the average lattice; this includes site occupation (short-range order scattering) as well as position (displacement scattering).[16–19]

For a binary solid solution $A-B$ of cubic structure, short-range order scattering in Laue units (Lu) is given by

$$I_{\mathrm{SRO}}(\mathbf{h}) = \sum_{lmn} \alpha_{lmn} \cos(\pi h_1 l)\cos(\pi h_2 m)\cos(\pi h_3 n), \quad (1)$$

where $\mathbf{h}=(h_1,h_2,h_3)$ is the scattering vector in reciprocal-lattice units (rlu) $2\pi/a$ (a=lattice parameter), and the α_{lmn} are the Warren-Cowley short-range order parameters[20] for neighboring shells with positions expressed by lmn (l,m,n in units of $a/2$ representing the type of neighbor). For a homogeneous solid solution, I_{SRO} is the monotonic Laue scattering (defined as one Laue unit).

Displacement scattering cannot be represented in closed form; following Borie and Sparks[21] it is commonly written in a series expansion. Its leading term is called size effect scattering or linear displacement scattering, in Laue units it is given by

$$I_{\mathrm{SE}}(\mathbf{h}) = \mathbf{h}\cdot\mathbf{Q}, \quad (2)$$

with, e.g.,

$$Q_x(\mathbf{h}) = \sum_{lmn} \gamma_{x,lmn} \sin(\pi h_1 l)\cos(\pi h_2 m)\cos(\pi h_3 n) \quad (3)$$

and

$$\gamma_{x,lmn} = -\mathrm{Re}\left\{\frac{f_A}{f_A - f_B}\right\} 2\pi\left(\frac{c_A}{c_B} + \alpha_{lmn}\right)\langle x_{lmn}^{AA}\rangle + \mathrm{Re}\left\{\frac{f_B}{f_A - f_B}\right\} 2\pi\left(\frac{c_B}{c_A} + \alpha_{lmn}\right)\langle x_{lmn}^{BB}\rangle. \quad (4)$$

The $\langle x_{lmn}^{\mu\mu}\rangle$, $\mu=A,B$ are the species-dependent static atomic displacements in units of the lattice parameter a, c_μ the atomic fractions, and f_μ the atomic scattering factors.

To recover the various contributions from the elastic diffuse scattering I_{diff}, several techniques are employed. While Borie and Sparks[21] neglected the species dependence of the static displacements (evaluation valid when using neutrons), Georgopoulos and Cohen[22] extended this approach to x rays allowing the species dependence of the static displacements to be recovered. Both approaches were employed in the present investigation.

B. First-principles calculations

The total energy of the competing phases Pt, $NiPt_7$, and $NiPt_3$ were calculated by the projector augmented wave (PAW) method[23,24] within the local-density approximation (LDA) (Refs. 25 and 26) as implemented in the Vienna *ab initio* simulation package (VASP).[27–29] The LDA was preferred as it works better than gradient approximations for the ground-state properties of Pt. It was also used by Sanati *et al.*[15] in their first-principles search of ground-state structures, where the $NiPt_7$ phase was found. The Brillouin-zone integration in the PAW calculations was performed by the tetrahedron method with Blöchl correction.[30] The plane-wave cutoff energy was set to 350 eV. To optimize the structure, the internal structural parameters were relaxed until the Hellmann-Feynman forces on each atom were negligible (<0.01 eV/Å). The PAW method was also employed to calculate strain-induced interactions.

The screened generalized perturbation method (SGPM) (Refs. 31–34) was used to obtain effective cluster interactions (ECI) parameters of an Ising-type Hamiltonian,

$$H_{\mathrm{conf}} = \frac{1}{4}\sum_p V_p^{(2)} \sum_{i,j\subset p} \sigma_i\sigma_j + \frac{1}{3}\sum_t V_t^{(3)} \sum_{i,j,k\subset t} \sigma_i\sigma_j\sigma_k + \frac{1}{4}\sum_q V_q^{(4)} \sum_{i,j,k,l\subset q} \sigma_i\sigma_j\sigma_k\sigma_l, \quad (5)$$

where $V_p^{(2)}$, $V_t^{(3)}$, and $V_q^{(4)}$ are the two-, three- and four-site interactions for the corresponding two-, three-, and four-site clusters denoted by p, t, and q. The σ_i are the occupation numbers taking on the values 1 or -1 if a Pt or a Ni atom occupies site i. The coefficient 1/4 in front of the pair interaction term is chosen to provide a consistent description with the ordering energy used in the evaluation of the effective pair interaction parameters from experiment.

In general, the ECI parameters are functions of composition, magnetic state, lattice spacing, and thus of temperature. Several contributions to the ECI parameters may be distinguished; a chemical contribution due to the dependence on the atomic configuration at (ideal) fixed lattice sites, a vibrational contribution due to the configurational dependence on thermal vibrations (see Ref. 35 for a review), and a contribution from local (beside global) lattice relaxations caused by changes in the symmetry of lattice sites due to the local environment. In this study the vibrational contribution was assumed to be relatively small and neglected. The chemical part of the ECI parameters was determined by Green's function Korringa-Kohn-Rostocker (KKR) calculations within

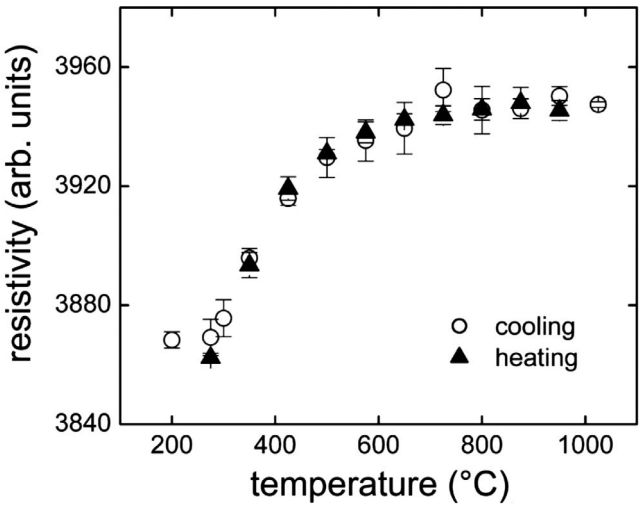

FIG. 2. Electrical-resistivity measurements of Ni-87.8 at. % Pt for a cooling and heating run. The values were taken at liquid-nitrogen temperature. The aging time at the indicated aging temperatures was 24 h.

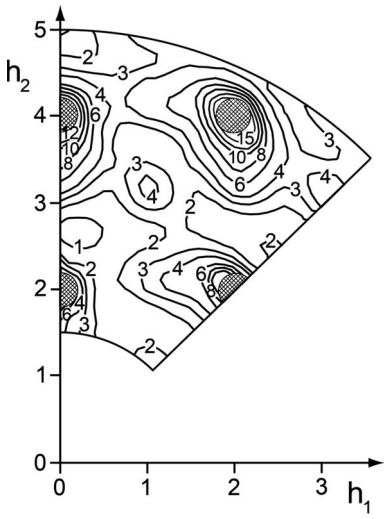

FIG. 3. Elastic and inelastic diffuse x-ray scattering of Ni-87.8 at. % Pt in Lu in the (001) plane. The hatched areas close to Bragg reflections indicate the regions with high intensity.

the atomic sphere (ASA) and coherent-potential approximations (CPA) (Ref. 36) using the SGPM (Refs. 33 and 34) with screened Coulomb interactions determined from the corresponding supercell calculations.[33] The contribution from lattice relaxations was determined in two ways; using two-site strain-induced interactions as obtained in total-energy calculations, as well as within the Krivoglaz-Khachaturyan formalism.[37,38]

III. EXPERIMENTAL

Ingots for crystal growing were produced by arc-melting and remelting in an induction furnace. They were prepared from 99.95 at. % pure Ni (Praxair MRC, Toulouse, France) and 99.98 at. % pure Pt (Johnson Matthey, London, United Kingdom).

A single crystal with a diameter of 11 mm was grown by electron-beam zone melting. A slice with diameter of 11 mm, thickness of 3 mm, and surface normal close to [9, 3, 2] was cut by spark erosion. The composition was Ni-87.8(3) at. % Pt as determined from x-ray fluorescence analysis using standards. The sample was finally polished with diamond powder of a grain size of 1 μm. It was then homogenized under Ar gas at 1373 K for 72 h, furnace cooled to 603 K where it was aged for 165 h, and cooled to room temperature in a stream of He gas. No mechanical surface treatment was subsequently applied as such a treatment was found to destroy single crystallinity, as revealed by weak Debye-Scherrer rings. An excellent surface is important, as the penetration depth is only $d=(2\mu)^{-1}=2.5$ μm (with μ=linear absorption coefficient, value for Mo $K\alpha$ radiation). The aging temperature was chosen following a sequence of resistivity measurements (cooling and heating run) of several samples (Fig. 2). For these measurements, the samples were quenched in brine water.

Elastic constants of a separate Ni-92.4 at. % Pt single crystal were determined using the pulse-echo-overlap method. The elastic constants of Ni-87.8 at. % Pt were obtained by linear interpolation using the values of pure Pt (Ref. 39), they are $c_{11}=331(2)$ GPa, $c_{12}=230(4)$ GPa, and $c_{44}=92(1)$ GPa. The total (static and dynamic) Debye-Waller factor $\exp[-2B(\sin\theta/\lambda)^2]$ was determined on the basis of the elastic constants c_{ij} and the lattice-parameter change with composition, giving $B=0.344\times10^{-2}$ nm^2.

Diffuse scattering was measured at room temperature with Mo $K\alpha$ radiation from a 12 kW Rigaku rotating anode. Data were taken at about 10100 positions (h_1,h_2,h_3). They are located on a grid of 0.1 rlu, with $h_1<h_2<h_3$ in the scattering-vector range of 1.5–5 rlu. Typical intensities were 2000–6000 counts per 4 min. Calibrations with polystyrene before and after the diffuse scattering experiment agreed within 0.8%.

Thermal diffuse scattering up to third order and Compton scattering[40] were calculated and subtracted. Atomic scattering factors and anomalous scattering factors were taken from Refs. 41 and 42.

IV. LOCAL ATOMIC ARRANGEMENT FROM DIFFUSE SCATTERING

Figure 3 shows raw data (elastic and inelastic scattering) in Lu in the (001) plane. While thermal diffuse scattering of first order and Huang scattering are responsible for the large intensity increase close to Bragg reflections, short-range order, and linear displacement scattering are recognized through the diffuse maxima at 100 positions and their shift from the Lifshitz position.

The elastic diffuse scattering was separated into the contributions stemming from short-range order and static atomic displacements using the Georgopoulos-Cohen (GC) and the Borie-Sparks (BS) separation techniques. In the GC evaluation, the typically 65 positions of any set of symmetry-equivalent positions (146 such sets were measured) could be separated with an R value better than 4%. This quality in

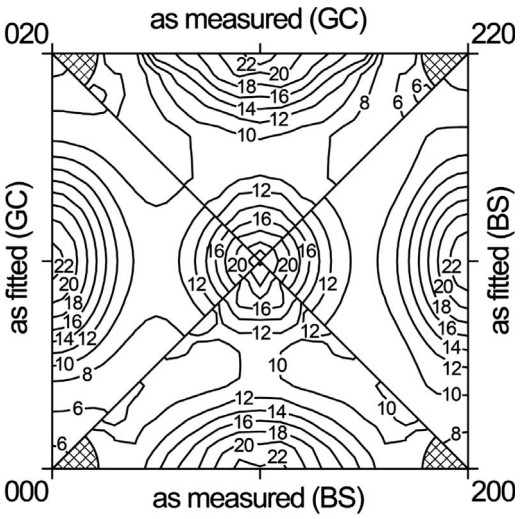

FIG. 4. Short-range order scattering $10\times I_{\mathrm{SRO}}(\mathbf{h})$ of Ni-87.8 at. % Pt in the (001) plane, for the as-separated and the fitted scattering using the Warren-Cowley short-range order parameters of Table I. The results are given for the Georgopoulos-Cohen and the Borie-Sparks evaluation.

fitting, however, was not achieved with the BS method for about 60 out of these 146 sets, all belonging to the *hhl* type. This failure is noticeable along ⟨110⟩ in Fig. 4 through the roughness of the separated short-range order scattering. As it is not noticed for *hk*0 positions, a pure reduction in the number of fitting parameters may not be responsible for this deficiency. However, there is one general problem with the BS evaluation and Ni-Pt alloys; the prefactor ratio $\mathrm{Re}\{\frac{f_A}{f_A-f_B}\}/\mathrm{Re}\{\frac{f_B}{f_A-f_B}\}$ assumed to be constant, varies by 26% within the range of scattering vectors, thus making the BS data uncertain in general, while this variation stabilizes the GC evaluation. No conclusion solely based on the present BS evaluation may be drawn, though a BS evaluation is often preferred over a GC evaluation because of the reduced number of fitting parameters (10 instead of 25 Fourier series have to be considered), especially if diffuse scattering is not much modulated.

A. Local order

Figure 4 shows short-range order scattering with diffuse maxima of about 2.3 Lu for both evaluations. Close to the Γ position, data tend to decrease toward about 0.6 Lu. Thus, there is local order. The Warren-Cowley short-range order parameters obtained from least-squares fitting are summarized in Table I. Not more than 12 parameters have to be considered to reach an *R* value of 3%–5%. For neighboring shells further away, the values of α_{lmn} get more and more comparable to the standard deviations that are solely based on counting statistics.

Table I shows that α_{000} is close to its theoretical value of 1. Uncertainties in input parameters—other than counting statistics—are presumably the reason, most probably it is calibration. The usually accepted uncertainty of ±5% in calibration introduces a variation by ±0.05 in α_{000}, while the present uncertainty in composition results in a variation by ±0.02. Note that for Ni-Pt alloys an uncertainty in calibration cannot be easily checked by considering the surroundings of Bragg positions where thermal diffuse scattering is the dominant scattering contribution: as Ni-Pt shows strong distortions (the lattice-parameter change with composition, $a^{-1}da/dc$, amounts to −0.078), Huang scattering close to Bragg positions will be large. With the present alloy, Huang scattering contributes about 50% of thermal diffuse scattering to the scattering in the close surroundings of Bragg reflections.

For the $\alpha_{lmn\neq 000}$, Table I provides a comparison with structures considered for possible ground states on the Pt-

TABLE I. Warren-Cowley short-range order parameters α_{lmn} for the Georgopoulos-Cohen and the Borie-Sparks evaluation of Ni-87.8 at. % Pt. In comparison, the parameters for the suggested adaptive structure $NiPt_7$ are shown, together with those expected for Ni-87.5 at. % Pt, if the $L1_2$ or $L1_0$ type of order were present.

	α_{lmn}				
lmn	GC	BS	$NiPt_7$	$L1_2$ type, $c=0.125$	$L1_0$ type, $c=0.125$
000	0.9208(41)	1.0783(27)	1.000	1.000	1.000
110	−0.0429(16)	−0.0230(12)	−0.143	−0.143	−0.048
200	0.0644(17)	0.0639(12)	0.619	0.429	0.143
211	−0.0274(10)	−0.0277(7)	−0.143	−0.143	−0.048
220	0.0347(11)	0.0345(8)	0.238	0.429	0.143
310	0.0005(08)	−0.0042(6)	−0.143	−0.143	−0.048
222	0.0026(13)	0.0004(8)	−0.143	0.429	0.143
321	−0.0009(5)	−0.0033(4)	−0.143	−0.143	−0.048
400	0.0078(15)	0.0027(10)	0.619	0.429	0.143
330	0.0067(10)	0.0057(7)	−0.143	−0.143	−0.048
411	−0.0043(9)	−0.0047(5)	0.238	−0.143	−0.048
420	0.0023(7)	0.0010(5)	0.238	0.429	0.143

TABLE II. Abundance analysis of nearest-neighbor configurations (Clapp configurations) with largest enhancement factors, for the short-range ordered state in the GC evaluation of Ni-87.8 at. % Pt and for the superstructures $NiPt_7$, $L1_2$, and $L1_0$. The nomenclature of the sites refers to Clapp (Ref. 45).

Structure	Clapp configuration	Sites occupied	Enhancement factor	Abundance in %
Ni around Pt				
SRO (GC)	C16	5,6,7,8	11.2	0.2
	C7	5,6,7	3.7	2.6
	C34	5,6,7,8,11	3.3	0.1
$NiPt_7$	C3	6,7		57.1
	C1			28.6
	C16	5,6,7,8		14.3
$L1_2$	C16	5,6,7,8		100
$L1_0$	C129	1,2,3,4,9,10,11,12		100
Ni around Ni				
SRO (GC)	C16	5,6,7,8	2.8	0.1
	C7	5,6,7	1.6	1.2
	C1		1.6	32.5
$NiPt_7$	C1			100
$L1_2$	C129	1,2,3,4,9,10,11,12		100
$L1_0$	C16	5,6,7,8		100

rich side of Ni-Pt; they are $NiPt_7$, $L1_2$, and $L1_0$. All of these structures exhibit a 100 superstructure reflection although the positions of diffuse maxima need not coincide with those of the superstructure reflections below the order-disorder transition temperature.[43] To normalize these structures to a common composition (a 1:7 stoichiometry was chosen), a Bragg-Williams approach of "gray" sublattices was adapted, and the α_{lmn} were taken to correspond to the maximum degree of order for the respective superstructure. Table I shows that the sign sequence of the α_{lmn} barely provides a means to discriminate among the structures. Only because of the signs of α_{222} and α_{411}, $L1_2$ and $L1_0$ are slightly favored over $NiPt_7$, while α_{330} of all three superstructures and the experimental value differ in sign. Still, "wrong" signs are well known to exist, e.g., for α_{211} in solid solutions and a nearby $L1_2$ ground state.[44]

An analysis in terms of Clapp configurations[45] is repeatedly taken as another means in the search for "fingerprints" of possible ground-state structures. Still, such an approach has to be considered with caution as diffuse scattering gives access to two-point correlations and not to thirteen-point correlations [central atom with its 12 (fcc) nearest neighbors, see also Ref. 46]. Two situations are listed in Table II. The first case (Ni atoms around any Pt atom) serves to indicate figures of $L1_2$ and $NiPt_7$, the second (Ni atoms around any Ni atom) those of $L1_0$ and $NiPt_7$. Clapp configurations with a high number (C129 in Table II) are not conclusive for the present case of a low degree of local order, as these configurations represent cases with many minority (Ni) atoms. A low running number in the Clapp configurations is not useful either for a detailed discussion of offstoichiometry certainly present with $L1_0$ and $L1_2$ because of the lower fraction of minority atoms (Ni atoms) in the present experiment. From the data in Table II, one reaches the following conclusions. The first case (Ni atoms around any Pt atom) points to $L1_2$ since a larger increase in the Clapp configurations of C1 and C3 (see their abundances in $NiPt_7$) is missing in the short-range ordered state, while C16 is strongest enhanced. However, all the short-range ordered states with C16 features and a known $L1_2$ ordered structure also showed C17 (indicator of an antiphase boundary between $L1_2$ type of domains, found, e.g., with Ni-rich Ni-Al and Ni-Ti, and Cu-rich Cu-Al and Cu-Au) making the present case unique. The second case (Ni atoms around a Ni atom) points to $L1_0$, known experimentally as a ground-state structure in Ni-Pt.

B. Static displacements

Static atomic displacements fitted to the separated displacement contributions, are summarized in Tables III and IV. As no radial approximation is employed (in contrast to Rodriguez *et al.*[7]), the number of fitted parameters remains limited in the present investigation. The recalculated contributions to I_{SE} are shown in Fig. 5. Two features are striking. (i) Displacements between Pt-Pt atoms are much smaller than those between Ni-Ni atoms. This outcome is expected as Pt atoms represent the majority component. (ii) Fig. 5 shows that the major modulations in the scattering contributions (at the low-angle side of a Bragg reflection) from Ni-Ni and Pt-Pt displacements have opposite signs. As

$$\mathbf{h}\cdot\mathbf{Q} = \mathrm{Re}\left\{\frac{f_{\mathrm{Ni}}}{f_{\mathrm{Ni}}-f_{\mathrm{Pt}}}\right\}\mathbf{h}\cdot\mathbf{Q}^{\mathrm{NiNi}} + \mathrm{Re}\left\{\frac{f_{\mathrm{Pt}}}{f_{\mathrm{Ni}}-f_{\mathrm{Pt}}}\right\}\mathbf{h}\cdot\mathbf{Q}^{\mathrm{PtPt}}, \tag{6}$$

TABLE III. Species-dependent [$\langle x_{lmn}^{\mathrm{PtPt}}\rangle$ and $\langle x_{lmn}^{\mathrm{NiNi}}\rangle$ from GC evaluation] and effective [$\gamma_{x,lmn}$ in the Georgopoulos-Cohen and Borie-Sparks evaluation] static atomic displacements of Ni-87.8 at. % Pt, in units of the lattice parameter a.

lmn	$\langle x_{lmn}^{\mathrm{PtPt}}\rangle$	$\langle x_{lmn}^{\mathrm{NiNi}}\rangle$	$\gamma_{x,lmn}$ (GC)	$\gamma_{x,lmn}$ (BS)
110	0.00182(36)	0.041(6)	−0.0912(27)	−0.0905(9)
200	0.00047(15)	0.068(14)	0.0137(123)	0.0067(77)
211	0.00055(3)	0.039(5)	−0.0173(26)	−0.0184(14)
121	0.00043(3)	0.012(5)	−0.0205(24)	−0.0188(18)
220	−0.00033(5)	0.000(5)	0.0195(41)	0.0207(15)
310	0.00013(4)	0.010(6)	−0.0028(34)	−0.0086(22)
130	−0.00006(4)	−0.009(5)	−0.0007(33)	−0.0038(19)
222	0.00008(1)	0.005(6)	−0.0027(36)	0.0011(19)

counterbalancing between both contributions may not be excluded.

To investigate this point further, two checks were performed. (i) Starting from the $\langle x_{lmn}^{\mathrm{PtPt}}\rangle$ and $\langle x_{lmn}^{\mathrm{NiNi}}\rangle$ of the GC evaluation, the $\gamma_{x,lmn}$ only accessible in a BS evaluation were calculated. A comparison of both sets for $\gamma_{x,lmn}$ (Table III) reveals close agreement. (ii) Using the elastic data of Pt, c_{11}=346.7 GPa, c_{12}=250.7 GPa, and c_{44}=76.5 GPa,[39] and a lattice-parameter change with composition of −0.078 for Ni in Pt, atomic displacements $\langle x_{lmn}^{\mathrm{PtNi}}\rangle$ were estimated in the dilute limit of Ni impurities within a Pt matrix using a continuum model introduced by Krivoglaz.[37] The situation is favorable for such a calculation as the elastic anisotropy $\xi=(c_{11}-c_{12}-2c_{44})/c_{44}=-0.75$ is small for Pt. The values of the radial displacements (i.e., shells 110, 200, 220, and 222) are comparable in magnitude ($10^{-3}a$) to those from the GC evaluation (Table IV). Thus, there is no compelling reason to evoke a compensating effect between the Ni-Ni and Pt-Pt displacements in evaluating the species-dependent scattering contributions.

TABLE IV. Species-dependent static atomic displacements $\langle x_{lmn}^{\mathrm{PtNi}}\rangle$ from diffuse scattering of Ni-87.8 at. % Pt and for the dilute limit of Ni in Pt based on Ref. 37 and from first-principles calculations using a 500-atom supercell, in units of the lattice parameter a.

	$\langle x_{lmn}^{\mathrm{PtNi}}\rangle$		
	Ni-87.8 at. % Pt	Dilute limit	
lmn	scattering	Ref. 37	Supercell
110	−0.0078(3)	−0.0079	−0.0081
200	−0.0096(18)	0.0002	−0.0010
211	−0.0042(3)		−0.0032
121	−0.0021(3)		−0.0021
220	0.0011(6)	−0.0036	−0.0010
310	−0.0012(5)		−0.0008
130	0.0009(4)		0.0002
222	−0.0006(5)	−0.0020	−0.0015

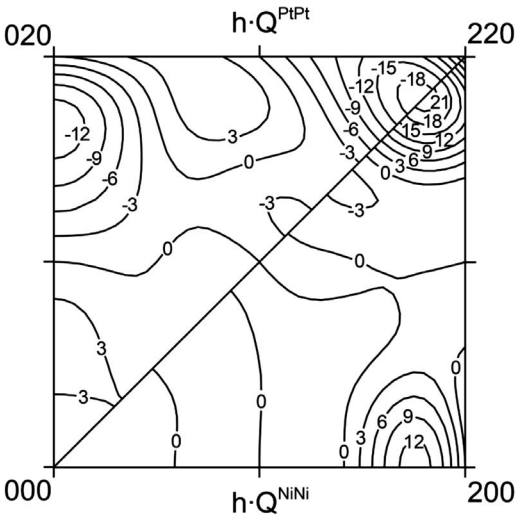

FIG. 5. Recalculated scattering $10\times\mathbf{h}\cdot\mathbf{Q}^{\mathrm{PtPt}}(\mathbf{h})$ and $10\times\mathbf{h}\cdot\mathbf{Q}^{\mathrm{NiNi}}(\mathbf{h})$ of Ni-87.8 at. % Pt in the (001) plane, using the fitted Fourier coefficients of Tables I and III for the Georgopoulos-Cohen evaluation.

V. INTERACTION PARAMETERS AND PHASE STABILITY

A. EPI parameters from diffuse scattering data

From the set of short-range order parameters α_{lmn} (Table I), effective pair interaction parameters were determined in two ways, by the inverse Monte Carlo (IMC) method[47] and by the Krivoglaz-Clapp-Moss (KCM) high-temperature approximation[37,48] including corrections for the first three neighboring shells as given by the γ-expansion method (GEM).[49] The ordering energy (per atom) in terms of the EPI parameters that correspond to the ECI parameters of Eq. (5), can be written as

$$E_{\mathrm{ord}}=c_Ac_B\sum_{lmn}V_{lmn}\alpha_{lmn}, \tag{7}$$

with $V_{lmn}=\frac{1}{2}(V_{lmn}^{AA}+V_{lmn}^{BB})-V_{lmn}^{AB}$. The EPI parameters in Eq. (7) will differ from the two-site ECI parameters of the same shell lmn [Eq. (5)] unless multisite interactions are negligible.[50]

For the IMC method, crystals with $48\times48\times48$ atoms and linear boundary conditions were employed. Data given in Table V were obtained as averages over five model crystals compatible with the α_{lmn} of Table I. The standard deviations are due to those of the α_{lmn}. The EPI parameters from KCM-GEM are also given in Table V. They were obtained using the Krivoglaz-Clapp-Moss equation,

$$I_{\mathrm{SRO}}(\mathbf{h})=\frac{C}{1+2c_Ac_B\tilde{V}(\mathbf{h})/(k_BT)}, \tag{8}$$

with normalization C=1 and $\tilde{V}(\mathbf{h})$=Fourier transform of the EPI parameters V_{lmn}, T=aging temperature, k_B=Boltzmann constant. A least-squares fitting employing the separated short-range order scattering and also a Fourier transforma-

TABLE V. EPI parameters V_{lmn} as determined from the sets of α_{lmn} of Ni-87.8 at. % Pt (Table I, GC evaluation). The inverse Monte Carlo method as well as the Krivoglaz-Clapp-Moss high-temperature approximation including the corrections by the γ-expansion method (KCM-GEM) were employed. Also given is the strain-induced contribution of the EPI parameters, V_{elast}.

	V_{lmn} (meV)		
lmn	IMC	KCM-GEM	V_{elast} (meV)
000		12.3(23)	
110	12.2(4)	9.7(11)	−43.7
200	−8.3(2)	−10.0(11)	−15.2
211	5.9(3)	4.9(8)	−1.9
220	−4.6(1)	−4.8(4)	2.8
310	−0.6(2)	−0.8(3)	−3.9
222	2.3(1)	2.5(4)	1.7
321	−0.6(1)	−0.4(2)	1.1
400	−0.2(2)	−0.5(5)	−2.6
330	−1.4(1)	−1.4(3)	2.4
411	−0.6(1)	−0.5(2)	−2.4
420	0.1(1)	0.0(2)	−1.1

tion employing the I_{SRO} recalculated from the α_{lmn} of Table I (ensuring $\alpha_{000}=1$) were done to determine the EPI parameters. The average of both evaluations is given in Table V. The standard deviations are due either to counting statistics or to the difference between both evaluations—the larger value was always taken. Note that the corrections for the three neighboring shells 110, 200, and 211 when employing the γ-expansion method are small, only comprising 0.06, 0.10, and 0.02 meV, respectively. The reason does not lie in the composition (corrections increase if the composition deviates from 1:1 stoichiometry, cf. Ref. 51), but in the low values of α_{lmn}. A good agreement between the IMC and KCM-GEM data sets is seen in Table V.

The number of EPI parameters obtainable from short-range order scattering is limited because of the limited range of the pair-correlation function that may be analyzed (Table I). This restriction might present a problem in the case of alloys with a large size effect as is the case with Ni and Pt.[11] Therefore, the purely elastic part to the EPI parameters was also determined following Khachaturyan.[38] Nearest-neighbor Kanzaki forces were calculated from the elastic constants c_{ij} of Ni-Pt and the lattice-parameter change with composition, yielding a value of -5.8×10^{-10} N, and the dynamical matrix was obtained from the elastic constants. This value is in good agreement with forces on the nearest-neighbor Pt atoms around a single Ni impurity in Pt obtained in the unrelaxed PAW first-principles calculations, which is -6.5×10^{-10} N (−0.405 eV/Å). Figure 6 shows good agreement with the experimental EPI parameters except for the first four shells where the chemical nature of the EPI parameters dominates. Monte Carlo (MC) simulations showed that the strain-induced part to the EPI parameters beyond the 11th shell (parameters up to shell index 800 were employed) could be added without much affecting the separated short-range order scattering.

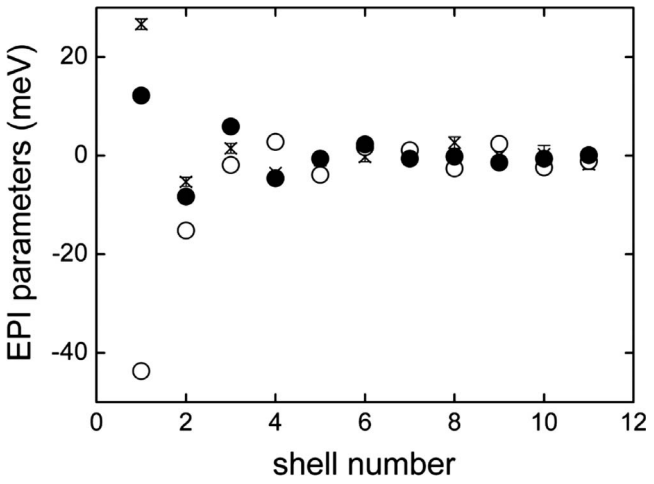

FIG. 6. EPI parameters for the first 11 shells for Ni-48 at. % Pt (Ref. 7, crosses) and for Ni-87.8 at. % Pt (this work, IMC evaluation, filled circles). In comparison, the strain-induced part of the EPI parameters, V_{elast}, for Ni-87.8 at. % Pt is also shown (Table V, open circles).

Monte Carlo simulations were performed in search of the suggested $NiPt_7$ ground-state structure of Ni-87.5 at. % Pt. Crystals of $16\times16\times16$ fcc unit cells and periodic boundary conditions were employed, compatible with the $L1_2$, $NiPt_7$, and $L1_0$ structures. The starting crystal represented either a random arrangement, a $NiPt_7$ structure or a state with a maximum degree of $L1_2$ order (Bragg-Williams order parameter of 0.5). Employing 18 000 MC steps, a two-phase microstructure of $NiPt_3$ (with $L1_2$ structure) within a Pt-rich matrix was always obtained, below 450(10) K for the IMC data set, 420(10) K for the KCM-GEM data set, and about 50(10) K lower when employing additionally the strain-induced contribution to the EPI parameters beyond the 11th shell.

Monte Carlo simulations were also performed to determine the order-disorder transition temperature for a possible $L1_2$ ground-state structure of Ni-75 at. % Pt. Starting from a crystal with either a random atomic arrangement or the $L1_2$ structure and using the EPI parameters from Table V (IMC and KCM-GEM data sets), a $L1_2$ structure was always obtained below an order-disorder transition temperature of 625(15) K. This result is not much changed when the strain-induced contribution to the EPI parameters beyond the 11th shell is added; the order-disorder transition temperature is only slightly lowered to 565(15) K.

These Monte Carlo simulations with Ni-75 at. % Pt and Ni-87.5 at. % Pt strongly support the presence of $NiPt_3$ with $L1_2$ structure, but not of $NiPt_7$.

B. Stability of $NiPt_7$ at 0 K from first-principles calculations

As the EPI parameters deduced from the diffuse scattering experiment correspond to a high-temperature alloy state, namely, the state at the annealing temperature, they cannot be used to give a definite answer about the ground-state

structure at 0 K. The reason is that the temperature dependence enters the EPI parameters (or ECI in general) in many ways; through lattice vibrations including thermal expansion, magnetic or other excitations. In this case, total-energy first-principles calculations may help, especially when the energy difference between competing structures is large compared with the error due to the approximations employed in such calculations.

The total energy of the totally relaxed structure of $NiPt_7$ was calculated for the atomic configuration suggested by Sanati *et al.*[15] and compared with the value of the competing phase separated state, consisting of pure Pt and $L1_2$-ordered $NiPt_3$; $\Delta H = E_{\mathrm{tot}}^{\mathrm{NiPt_7}} - E_{\mathrm{tot}}^{\mathrm{NiPt_3}} - 4E_{\mathrm{tot}}^{\mathrm{Pt}}$, where the energy is per elementary unit cell. The structures were first relaxed using a Monkhorst-Pack k-point mesh,[52] that corresponds to a $40 \times 40 \times 40$ grid of the fcc Brillouin zone. Then the total energies of the relaxed structures were calculated using the tetrahedron method without smearing the electron spectrum with the Blöchl correction.[30] In the nonmagnetic (NM) calculations $\Delta H = 1.1$ meV/cell (0.13 meV/atom) is obtained. Although ΔH is positive, which means that $NiPt_7$ is not stable, no definite conclusion may be drawn from such a small value. In the magnetic calculations, Ni atoms acquire a magnetic moment of about $0.5\mu_B$ (μ_B=Bohr magneton) in $NiPt_7$ and $NiPt_3$, and this leads to $\Delta H = 11.5$ meV/cell (1.44 meV/atom) and a pronounced destabilization of $NiPt_7$. Thus, the first-principles calculations do not predict the stability of $NiPt_7$, although the energy difference is still very small, and, of course, there is no guarantee that, e.g., a better treatment of the exchange-correlation energy will reverse the result. Note that the authors do not know exactly why $NiPt_7$ has been found stable in similar *ab initio* calculations in Ref. 15 since the details of calculations are not given. One can only speculate that it was due to the use of an ultrasoft pseudopotential method, which is usually less accurate for transition metals and alloys than the PAW method used in the present work.

C. ECI parameters from first-principles calculations

EPI parameters as determined from diffuse scattering experiments depend on aging temperature and may effectively include multisite interactions. Therefore, pair, three-, and four-site interactions in a random Ni-87.5 at. % Pt alloy were calculated using first-principles methods. In particular, the SGPM method was employed to get the chemical part of the ECI, i.e., the interactions on a fixed underlying lattice. Since the interactions at the first few coordination shells are most sensitive to the errors due to CPA and ASA, the locally self-consistent Green's function (LSGF) method was also used to calculate the effective pair interactions at the first four coordination shells from the total energies of Ni-87.5 at. % Pt using 864-atom supercells.

The atomic configuration of these supercells has been prepared in such a way that they had only one non-negligible short-range order parameter, α_p, at the coordination shell p within the first eight coordination shells of the fcc lattice. Then, if the local interaction zone in the LSGF method includes coordination shell p, the effective pair interaction at this coordination shell is $\Delta E_p / c(1-c)\alpha_p z_p$, where ΔE_p is the difference of the total energies (per atom) of a supercell with nonzero short-range order parameter at coordination shell p and a supercell of a completely random alloy, and z_p the coordination number at coordination shell p.

TABLE VI. Chemical (V_{ch}) and strain-induced (V_{si}) part to the ECI parameters $V_p^{(2)}$ of Ni-87.5 at. % Pt, together with $V_{\mathrm{tot}} = V_{\mathrm{ch}} + V_{\mathrm{si}}$. While V_{ch} was calculated by the LSGF approach for the first four shells, two approaches were chosen for the subsequent shells: V_{ch} was obtained by the SGPM in the nonmagnetic as well as (values in parenthesis) disordered local-moment state with longitudinal spin fluctuations at 600 K.

lmn	V_{ch} (meV)	V_{si} (meV)	V_{tot} (meV)
110	64.62	−54.7	9.9
200	1.99	−29.1	−27.1
211	−1.80	−2.6	−4.4
220	−5.85	1.7	−4.2
310	0.84 (0.76)		
222	2.14 (2.35)		
321	0.39 (0.36)		
400	0.39 (0.47)		
330	−1.54 (−2.08)		
411	0.00 (−0.01)		
420	0.28 (0.27)		

To consider thermal lattice expansion at 600 K, the calculations were done for a lattice constant of 3.89 Å, slightly higher than the experimental value of 3.885 Å at room temperature.[53] The other thermal excitation effect, which has been suspected to play some role, is finite-temperature magnetism. The calculations show that the magnetic moment of a Ni atom remains nonzero in both the ferromagnetic state ($0.63\mu_B$) and the disordered local moment (DLM) state ($0.42\mu_B$), which is a simple mean-field model of the paramagnetic state.[54] Note that in pure Ni, the local magnetic moment disappears in the DLM state at 0 K. Although the local magnetic moment on Pt atoms in Ni-87.5 at. % Pt vanishes in the DLM state at zero K, it has a finite value at elevated temperature due to temperature-induced longitudinal spin fluctuations (LSF). The estimations using the formalism developed in Ref. 55 show, that its value is about $0.39\mu_B$ at 600 K. The LSF also increase the local magnetic moment on Ni atoms up to about $0.77\mu_B$. In spite of quite substantial values of the local magnetic moments, the ECI parameters obtained by SGPM in the DLM state with LSF at 600 K are very close to those in the nonmagnetic calculations. Thus, the finite-temperature magnetism has little effect on the ECI parameters, at least for this particular alloy composition at 600 K.

In Table VI the values of the ECI parameters, $V_p^{(2)}$, as determined in the first-principles calculations are summarized. In the first column, the chemical contribution V_{ch} is provided: the parameters at the first four coordination shells are obtained by the LSGF method, as described above, and at the other shells in the SGPM nonmagnetic calculations (the

parameters in the DLM state with the LSF at 600 K are given in parenthesis). To check the accuracy of the effective chemical interactions, the ordering energy was calculated for 13 assumed superstructures for Ni-87.5 at. % Pt on a fixed (unrelaxed) fcc lattice. The largest error amounted to about 4 meV/atom for the Pt_7Cu type of structure, while the rest (built upon three different 16-atom supercells) was only about 1 meV, which indicates that the chemical interactions are of reasonable accuracy.

In the second column of Table VI, the strain-induced contribution to $V_p^{(2)}$, V_{si}, is given, which has been calculated from first principles in the dilute limit of Ni in Pt at the equilibrium lattice spacing of Pt, 3.905 Å. The results were obtained from total-energy calculations of a 256-atom supercell (a $4\times4\times4$ supercell, built on a four-atom fcc cell) consisting of a Ni pair in Pt and a single Ni atom, respectively,

$$V_{si} = \Delta E_{rel}^{Ni-Ni} - 2\Delta E_{rel}^{Ni}. \quad (9)$$

Here, ΔE_{rel}^{Ni-Ni} and ΔE_{rel}^{Ni} are the local relaxation energies of a Ni pair and a single Ni atom, respectively, in Pt (the volume and the geometry of the supercell are kept fixed). A comparison between V_{elast} of Table V and V_{si} of Table VI shows a reasonable qualitative agreement, although the first-principles value of the V_{si} for the second coordination shell is apparently much lower.

In Table IV the species-dependent atomic displacements $\langle x_{lmn}^{PtNi}\rangle$ as obtained in the supercell calculations of a single Ni atom in Pt are also shown. Additional 500-atom supercell calculations performed to check the convergence with the size of the supercell, indicated a 10% variation with size. Comparing these results with the experimental data, one can see that there is very good agreement for displacements between Ni and Pt atoms at the first three coordination shells.

The sum of the chemical and strain-induced contributions, V_{tot}, is listed in the last column of Table VI and can be compared with the EPI parameters from diffuse scattering (Table V). Again, the agreement is qualitatively reasonable, with a substantial difference for the second coordination shell, which turns out to be very low in the first-principles calculations due to large negative contributions from the strain-induced interactions. Monte Carlo simulations with these first-principles interactions produce a phase separation into $NiPt_3$ with $L1_2$ structure and Pt at about 600 K, which makes it impossible to compare the theoretical and experimental values of the short-range order parameters at 600 K.

Although, the contributions from phonons have been neglected, we believe that the major problem in these calculations comes from the approximate way in which the strain-induced interactions are considered. It is clear that the strain-induced interactions, being directly connected to the local symmetry of the sites, can be largely affected by the underlying short-range order and the fluctuations of composition in random alloys. This means that some of them can vary quite largely in real random alloys, compared to the dilute limit. More investigations are required, but this is beyond the scope of the present paper.

Finally, according to the GPM calculations, the multisite interactions are relatively small in Ni-87.5 at. % Pt. In particular, the strongest three-site interaction parameter (for the three nearest-neighbor sites along one ⟨110⟩ direction) is only −1.4 meV. The three-site interaction for the triangle of nearest neighbors is about −0.5 meV. All the other three-site parameters are less than 0.1 meV in magnitude, and may be neglected in the configurational thermodynamics at all. This is also true for the four-site interaction parameters; the strongest parameter is for the tetrahedron of nearest neighbors, amounting to 0.07 meV. This means that the EPI solely determine the configurational energetics of the system, and therefore the EPI obtained in the experiment can in principle be used as a benchmark for theoretical calculations, provided that the problem with a long-range tail of the strain-induced interactions is solved. Note that the considerable number of sizable three-site and four-site interactions for Ni-Pt in Ref. 15 is due to the cluster expansion of the enthalpies of formation of ordered alloys in the whole concentration range. For a *fixed* concentration and a *fixed* volume, they are in fact small.

VI. STABILITY OF $NiPt_3$

To the authors' knowledge, no details of experimental investigations on $NiPt_3$ were provided yet, only some order-disorder transition temperatures off the 1:3 stoichiometry were given (Refs. 3 and 4), but these data were not included in the phase diagram handbooks of Massalski.[5]

Using the EPI parameters from diffuse scattering, the above Monte Carlo simulations showed a decomposition of Ni-87.5 at. % Pt into a $L1_2$ particle within a matrix that consists nearly exclusively of Pt atoms at a low temperature of 300 K. This is an indication but no proof for the existence of $NiPt_3$ with $L1_2$ structure, as no energy of mixing is considered in these Monte Carlo simulations. The presence of the $L1_2$ superstructure is also supported by the present total-energy calculations that demonstrated an instability of an assumed $NiPt_7$ structure with respect to decomposition into $NiPt_3$ and Pt at 0 K.

To examine the presence of $NiPt_3$, two types of experiments were performed; electrical resistivity was measured that will indicate strong changes in the atomic arrangement, and x-ray scattering across superstructure positions that will provide insight into the type of superstructure.

Electrical resistivity was investigated for Ni-75 at. % Pt in a cooling and heating run, similar to those presented for Ni-87.8 at. % Pt in Fig. 2. With aging times of 24 h, the possibility for setting up a state of thermal equilibrium and freezing it in quenching was noted for the temperature range 720–900 K. However, slight differences between the heating and cooling run below 720 K indicated the need for longer aging time. For this to overcome, aging at 1120 K and a subsequent quenching to room temperature were performed just prior to any aging below 670 K, i.e., more vacancies were provided in the start of the ordering process. Now a drastic decrease (by some 10%) in electrical resistivity even within 24 h of aging was noted, indicating the appearance of long-range order. Such a large decrease is comparable in magnitude to those given by Leroux *et al.*[56] when lowering the temperature to get from locally ordered to the long-range ordered states of Ni_3Pt and NiPt.

Superstructure reflections of a single crystal of Ni-75.2(5) at. % Pt were exclusively seen at *hkl* (with h,k,l not all even or all odd) positions, as expected for $L1_2$. The degree of long-range order was determined by comparing integrated intensities of superstructure and fundamental reflections, corrected for the angle-dependent factors of structure factor, Debye-Waller factor, and polarization. For aging at 630 K, a value of $\eta=0.3(1)$ was obtained. Also considering the strong decrease in electrical resistivity below 670 K, an order-disorder transition temperature of 650(20) K is estimated for Ni-75 at. % Pt.

VII. DISCUSSION

Interaction parameters from electronic-structure calculations or diffuse scattering experiments may always be submitted a test how closely they reproduce experimentally known order-disorder transition temperatures. In Ni-Pt this may be performed for Ni-50 at. % Pt. ECI parameters determined from electronic-structure calculations[2,12,14] always showed a leading nearest-neighbor value among the first four EPI parameters usually reported. Pourovskii *et al.*[2] found that the first four EPI parameters are sufficient for determining the ordering energy, and 900 to 950 K was obtained for the order-disorder transition temperature of the $L1_0$ structure. This value is close to the experimental data of 918 K. Based on the experimental EPI parameters of Rodriguez *et al.*,[7] a transition temperature may be determined, applying Monte Carlo simulations. This yields a value of 1000(20) K, slightly higher than 918 K. Usually, when a noncubic to cubic transition was estimated by such simulations [the $L1_0$ structure of NiPt has a tetragonality c/a of about 0.94 (Ref. 53)], a distinctly lower value was obtained.[18] This underestimate was rationalized by the expectation that the structural change in the ordered phase contributes to its stabilization. The present agreement with the experimental value is excellent in both approaches, and one might hope for a similar quality of agreement for $NiPt_3$.

The leading EPI parameters of Ni-87.8 at. % Pt (Table V) are smaller than those reported by Rodriguez *et al.*[7] for Ni-48 at. % Pt. This is reflected in the above comparison where the phase stability of $NiPt_3$ was estimated. This dependence on composition is consistent with electronic-structure calculations by Paudyal *et al.*,[14] where a decrease in the nearest-neighbor EPI parameter with increasing Pt fraction was the most obvious change.

Knowledge of ground-state energies is required to discuss phase stability at 0 K. From diffuse scattering, only the configurational part may be estimated. Figure 7 shows ordering energies determined with the EPI parameters of this work (connected by solid line) and of Rodriguez *et al.*[7] (connected by dashed line). A stability of $NiPt_3$ and no stability for $NiPt_7$ are suggested. The difference in the ordering energy of $NiPt_3$ (with $L1_2$ structure) determined from both data sets reflects the composition dependence of the EPI parameters. This dependence assists in destabilizing $NiPt_7$, while a convex shape of the energy of mixing[57] works oppositely. Still, there is a decisive point to be noted as calculations (as well as diffuse scattering) were performed just for Ni-87.5 at. % Pt, even if

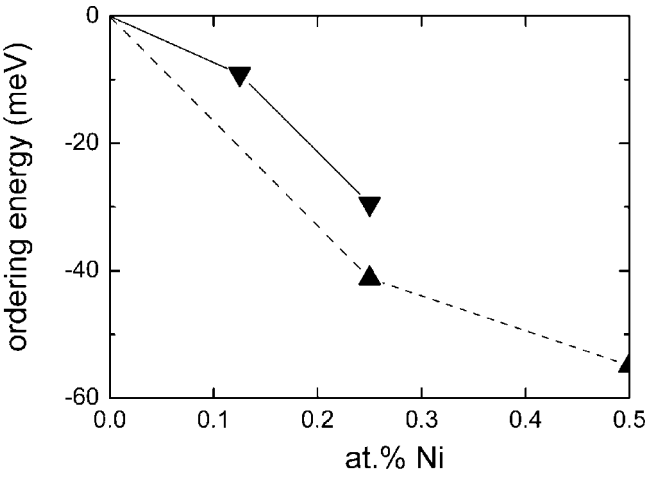

FIG. 7. Ordering energies for $NiPt_7$ and $NiPt_3$ ($L1_2$) using the IMC data of Table V (triangles down) and $NiPt_3$ ($L1_2$) and NiPt ($L1_0$) with the EPI parameters from Rodriguez *et al.* (Ref. 7) (triangles up). Lines are drawn to guide the eyes.

the configurational part of the energy is only determined: if the $NiPt_7$ superstructure is unstable in Monte Carlo simulations, then $NiPt_7$ is indeed unstable, irrespective of what will be the final state.

Considering Ni-75 at. % Pt good agreement on the order-disorder transition temperature is found among the various data. While the EPI parameters from diffuse scattering of Ni-87.8 at. % Pt give a value of 625(15) K [and 565(15) K when the strain-field contribution at large distances is tentatively incorporated], the direct experimental investigations of Ni-75 at. % Pt give 650(20) K. This result is also in excellent agreement with the 720 K obtained by extrapolating the dotted line in Refs. 3 and 4 to Ni-75 at. % Pt.

Values of static atomic displacements in Ni-Pt alloys are barely found in the literature and were not yet provided by experiments, as so far evaluations of the Borie-Sparks type were employed.[6,7] Based on electronic-structure calculations, there is one data set[58] on nearest-neighbor displacements in a Ni-50 at. % Pt random alloy, with $\langle x_{110}^{\mathrm{PtPt}}\rangle > 0$, $\langle x_{110}^{\mathrm{NiPt}}\rangle < 0$, and $\langle x_{110}^{\mathrm{NiNi}}\rangle < 0$. Based on the bond lengths within the spring model of Ref. 58, $\gamma_{x,110}=-0.022$ is expected, instead of the experimental value of 0.047.[7] Differences, however, might easily occur; in the experiment displacements were only approximately considered by the radial approximation and in the calculations a random and not a short-range ordered state was considered. It is well known that the displacements depend on the actual local atomic arrangement. This was noted for a solid solution of Ni-rich Ni-Al, following molecular-dynamics simulations.[59]

VIII. CONCLUSIONS

Diffuse x-ray scattering of Ni-87.8 at. % Pt and *ab initio* electronic structure calculations are done to provide evidence for the ground-state structures at the Pt-rich side of Ni-Pt. Based on total-energy calculations at 0 K and Monte Carlo

simulations with EPI parameters from diffuse scattering, no compelling reason is found that there is the suggested adaptive superstructure $NiPt_7$. Instead of it, evidence is noted for the ordered $NiPt_3$ state with $L1_2$ superstructure based on Monte Carlo simulations and the presence of superstructure reflections for Ni-75.2 at. % Pt. This phase is missing in the current phase diagrams and should be added. Good agreement between diffuse scattering and electronic structure calculations is also found for the interaction parameters and the static atomic displacements between nearest neighbors.

ACKNOWLEDGMENTS

The authors are grateful to E. Fischer for his support in growing the single crystals. B.S. and M.E. also thank J. Löffler for his support and encouragement. This work was partially supported by the "Schweizerischer Nationalfonds zur Förderung der wissenschaftlichen Forschung." A.V.R. acknowledges financial support by the Swedish Foundation for Strategic Research (SSF) and the Swedish Research Council (VR).

[1] Y. Gauthier, Surf. Rev. Lett. **3**, 1663 (1996).
[2] L. V. Pourovskii, A. V. Ruban, I. A. Abrikosov, Y. Kh. Vekilov, and B. Johansson, Phys. Rev. B **64**, 035421 (2001).
[3] C. E. Dahmani, M. C. Cadeville, J. M. Sanchez, and J. L. Morán-López, Phys. Rev. Lett. **55**, 1208 (1985).
[4] M. C. Cadeville, C. E. Dahmani, and F. Kern, J. Magn. Magn. Mater. **54-57**, 1055 (1986).
[5] T. B. Massalski, *Binary Alloy Phase Diagrams* (ASM International, Materials Park, Ohio, 1990).
[6] D. K. Saha and K.-i Ohshima, J. Phys.: Condens. Matter **7**, 3203 (1995).
[7] J. A. Rodriguez, S. C. Moss, J. L. Robertson, J. R. D. Copley, D. A. Neumann, and J. Major, Phys. Rev. B **74**, 104115 (2006).
[8] D. K. Saha and K.-i. Ohshima, J. Phys.: Condens. Matter **5**, 4099 (1993).
[9] C. E. Dahmani, M. C. Cadeville, and V. Pierron-Bohnes, Acta Metall. **33**, 369 (1985).
[10] F. J. Pinski, B. Ginatempo, D. D. Johnson, J. B. Staunton, G. M. Stocks, and B. L. Gyorffy, Phys. Rev. Lett. **66**, 766 (1991).
[11] Z. W. Lu, S.-H. Wei, and A. Zunger, Europhys. Lett. **21**, 221 (1993).
[12] P. P. Singh, A. Gonis, and P. E. A. Turchi, Phys. Rev. Lett. **71**, 1605 (1993).
[13] A. V. Ruban, I. A. Abrikosov, and H. L. Skriver, Phys. Rev. B **51**, 12958 (1995).
[14] D. Paudyal, T. Saha-Dasgupta, and A. Mookerjee, J. Phys.: Condens. Matter **15**, 1029 (2003).
[15] M. Sanati, L. G. Wang, and A. Zunger, Phys. Rev. Lett. **90**, 045502 (2003).
[16] G. Kostorz, in *Physical Metallurgy*, 4th ed., edited by R. W. Cahn and P. Haasen (North-Holland, Amsterdam, 1996), p. 1115.
[17] W. Schweika, *Disordered Alloys: Diffuse Scattering and Monte-Carlo Simulations, Springer Tracts in Modern Physics No. 141* (Springer, Berlin, 1998).
[18] B. Schönfeld, Prog. Mater. Sci. **44**, 435 (1999).
[19] G. E. Ice and C. J. Sparks, Annu. Rev. Mater. Sci. **29**, 25 (1999).
[20] J. M. Cowley, J. Appl. Phys. **21**, 24 (1950).
[21] B. Borie and C. J. Sparks, Jr., Acta Crystallogr. A **27**, 198 (1971).
[22] P. Georgopoulos and J. B. Cohen, J. Phys. (Paris), Colloq. **38**, C7–191 (1977).
[23] G. Kresse and D. Joubert, Phys. Rev. B **59**, 1758 (1999).
[24] P. E. Blöchl, Phys. Rev. B **50**, 17953 (1994).
[25] W. Kohn and L. J. Sham, Phys. Rev. **140**, A1133 (1965).
[26] J. P. Perdew and Y. Wang, Phys. Rev. B **45**, 13244 (1992).
[27] G. Kresse and J. Hafner, Phys. Rev. B **48**, 13115 (1993).
[28] G. Kresse and J. Furthmüller, Comput. Mater. Sci. **6**, 15 (1996).
[29] G. Kresse and J. Furthmüller, Phys. Rev. B **54**, 11169 (1996).
[30] P. E. Blöchl, O. Jepsen, and O. K. Andersen, Phys. Rev. B **49**, 16223 (1994).
[31] F. Ducastelle and F. Gautier, J. Phys. F: Met. Phys. **6**, 2039 (1976).
[32] F. Ducastelle, *Order and Phase Stability in Alloys* (North-Holland, Amsterdam, 1991).
[33] A. V. Ruban and H. L. Skriver, Phys. Rev. B **66**, 024201 (2002); A. V. Ruban, S. I. Simak, P. A. Korzhavyi, and H. L. Skriver, *ibid.* **66**, 024202 (2002).
[34] A. V. Ruban, S. Shallcross, S. I. Simak, and H. L. Skriver, Phys. Rev. B **70**, 125115 (2004).
[35] A. van de Walle and G. Ceder, Rev. Mod. Phys. **74**, 11 (2002).
[36] A. V. Ruban and H. L. Skriver, Comput. Mater. Sci. **15**, 119 (1999).
[37] M. A. Krivoglaz, *X-ray and Neutron Diffraction in Nonideal Crystals* (Springer, Berlin, 1996); *Diffuse Scattering of X-rays and Neutrons by Fluctuations* (Springer, Berlin, 1996).
[38] A. G. Khachaturyan, *Theory of Structural Transformations in Solids* (Wiley, New York, 1983).
[39] R. E. MacFarlane, J. A. Rayne, and C. K. Jones, Phys. Lett. **18**, 91 (1965).
[40] D. T. Cromer, J. Chem. Phys. **50**, 4857 (1969).
[41] *International Tables for Crystallography*, edited by A. J. C. Wilson (Kluwer, Dordrecht, 1992).
[42] S. Sasaki, KEK Report No. 88–14, KEK, Tsukuba, Japan, 1989 (unpublished).
[43] Z. W. Lu and A. Zunger, Phys. Rev. B **50**, 6626 (1994).
[44] U. Gahn and W. Pitsch, Acta Metall. **37**, 2455 (1989).
[45] P. C. Clapp, Phys. Rev. B **4**, 255 (1971).
[46] D. M. C. Nicholson, R. I. Barabash, G. E. Ice, C. J. Sparks, J. L. Robertson, and C. Wolverton, J. Phys.: Condens. Matter **18**, 11585 (2006).
[47] V. Gerold and J. Kern, Acta Metall. **35**, 393 (1987).
[48] P. C. Clapp and S. C. Moss, Phys. Rev. **142**, 418 (1966).
[49] I. V. Masanskii, V. I. Tokar, and T. A. Grishchenko, Phys. Rev. B **44**, 4647 (1991).
[50] C. Wolverton, A. Zunger, and B. Schönfeld, Solid State Commun. **101**, 519 (1997).
[51] L. Reinhard and S. C. Moss, Ultramicroscopy **52**, 223 (1993).
[52] H. J. Monkhorst and J. D. Pack, Phys. Rev. B **13**, 5188 (1976).
[53] W. B. Pearson, *A Handbook of Lattice Spacings and Structures*

of Metals and Alloys (Pergamon Press, New York, 1958).
[54] B. L. Gyorffy, A. J. Pindor, J. B. Staunton, G. M. Stocks, and H. Winter, J. Phys. F: Met. Phys. **15**, 1337 (1985).
[55] A. V. Ruban, S. Khmelevskyi, P. Mohn, and B. Johansson, Phys. Rev. B **76**, 014420 (2007).
[56] C. Leroux, M. C. Cadeville, V. Pierron-Bohnes, G. Inden, and F. Hinz, J. Phys. F: Met. Phys. **18**, 2033 (1988).
[57] *Phase Diagrams of Binary Nickel Alloys*, edited by P. Nash (ASM International, Materials Park, Ohio, 1991).
[58] A. V. Ruban, S. I. Simak, S. Shallcross, and H. L. Skriver, Phys. Rev. B **67**, 214302 (2003).
[59] B. Schönfeld, G. Kostorz, M. Celino, and V. Rosato, Europhys. Lett. **54**, 482 (2001).